Journal of Inorganic Biochemistry 160 (2016) 210–217

Contents lists available at ScienceDirect

Journal of Inorganic Biochemistry

journal homepage: www.elsevier.com/locate/jinorgbio

A novel dual-functioning ruthenium(II)–arene complex of an anti-microbial ciprofloxacin derivative — Anti-proliferative and anti-microbial activity

Ziga Ude [a], Isolda Romero-Canelón [b], Brendan Twamley [c], Deirdre Fitzgerald Hughes [d], Peter J. Sadler [b,*], Celine J. Marmion [a,*]

[a] Centre for Synthesis and Chemical Biology, Department of Pharmaceutical & Medicinal Chemistry, Royal College of Surgeons in Ireland, 123 St. Stephen's Green, Dublin 2, Ireland
[b] Department of Chemistry, University of Warwick, Coventry CV4 7AL, UK
[c] School of Chemistry, Trinity College Dublin, Dublin 2, Ireland
[d] Department of Clinical Microbiology, Royal College of Surgeons in Ireland, Dublin, Ireland

ARTICLE INFO

Article history:
Received 7 October 2015
Received in revised form 22 January 2016
Accepted 10 February 2016
Available online 11 February 2016

Keywords:
Ruthenium(II)
Ruthenium(II)–arene
Ciprofloxacin
Anti-cancer
Anti-microbial
Crystal structure

ABSTRACT

7-(4-(Decanoyl)piperazin-1-yl)-ciprofloxacin, CipA, (**1**) which is an analogue of the antibiotic ciprofloxacin, and its ruthenium(II) complex [Ru(η^6-*p*-cymene)(CipA$_H$)Cl], (**2**) have been synthesised and the x-ray crystal structures of **1**·1.3H_2O·0.6CH_3OH and **2**·CH_3OH·0.5H_2O determined. The complex adopts a typical pseudo-octahedral 'piano-stool' geometry, with Ru(II) π-bonded to the *p*-cymene ring and σ-bonded to a chloride and two oxygen atoms of the chelated fluoroquinolone ligand. The complex is highly cytotoxic in the low μM range and is as potent as the clinical drug cisplatin against the human cancer cell lines A2780, A549, HCT116, and PC3. It is also highly cytotoxic against cisplatin- and oxaliplatin-resistant cell lines suggesting a different mechanism of action. The complex also retained low μM cytotoxicity against the human colon cancer cell line HCT116p53 in which the tumour suppressor p53 had been knocked out, suggesting that the potent anti-proliferative properties associated with this complex are independent of the status of p53 (in contrast to cisplatin). The complex also retained moderate anti-bacterial activity in two *Escherichia coli*, a laboratory strain and a clinical isolate resistant to first, second and third generation β-lactam antibiotics.

1. Introduction

The rational design and development of innovative anti-cancer platinum drug candidates to overcome dose-limiting toxic side effects and resistance associated with drugs in clinical use have produced a wide range of possible chemotherapeutics. However, in the 50 or so years since the discovery of the anti-cancer properties of cisplatin, it is surprising that none to date has been as successful as cisplatin and its analogues carboplatin or oxaliplatin. Recent advances in this field have included the exploitation of various Pt drug delivery vehicles [1] and the incorporation of metals other than Pt. In the latter regard, ruthenium compounds have demonstrated much promise with three Ru(III) complexes, NAMI-A (imidazolium *trans*-[tetrachloro(dimethylsulfoxide)(1*H*-imidazole)ruthenate(III)]) [2,3], KP1019 (indazolium *trans*-[tetrachlorobis(*1H*-indazole)-ruthenate(III)]) [4–6] and NKP-1339, the sodium salt analogue of KP1019 [4], all undergoing clinical trials, Fig. 1. Ruthenium(III) complexes tend to be less toxic, and may mimic the behaviour of iron in the body, taking advantage of transferrin-mediated delivery to cancer cells. Ruthenium(III) complexes may also act as prodrugs, being reduced to and exerting their biological effect as Ru(II) in the more reducing environment of tumour cells.

Half-sandwich Ru(II)–arene complexes provide a versatile platform for the design of anti-cancer complexes. For example, these complexes can be rationally designed such that they incorporate various biologically-relevant ligands or substituents, or ligands that serve to enhance the physicochemical properties of the complex, thus potentially leading to innovative multi-functional drug candidates. One property of potential value in the setting of cancer is anti-bacterial activity, given the weakened ability of patients with cancer to fight infection. A multitude of Ru–arene-type complexes with promising anti-cancer activity have been developed several of which target the nucleobases of DNA, for example, [(Ru-*p*-cymene)(ethylenediamine)Cl]PF_6 (RAED-C, Fig. 1), which is as cytotoxic as cisplatin [7–9]. The structurally-related anti-metastatic and anti-angiogenic agent [(Ru-*p*-cymene)(1,3,5-triaza-7-phosphaadamantane)Cl_2] (RAPTA-C, Fig. 1), in contrast,

* Corresponding authors.
E-mail addresses: P.J.Sadler@warwick.ac.uk (P.J. Sadler), cmarmion@rcsi.ie (C.J. Marmion).

http://dx.doi.org/10.1016/j.jinorgbio.2016.02.018

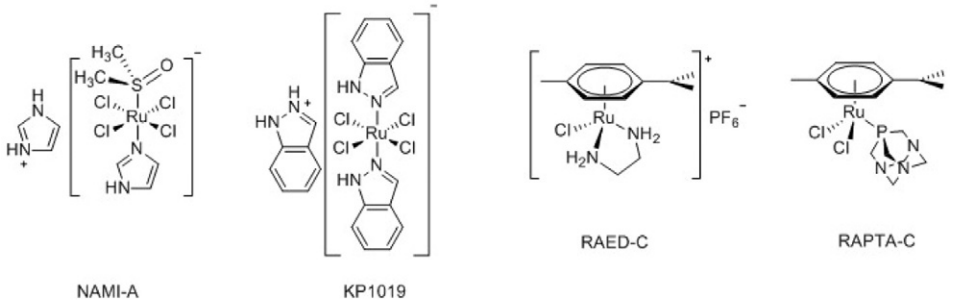

Fig. 1. Chemical structures of NAMI-A, KP1019, RAED-C and RAPTA-C.

accumulates on cellular chromatin forming adducts with core nucleosomal histone proteins [9].

Ruthenium(II) arene complexes incorporating clinical drugs such as ethacrynic acid (a gluthathione-S-transferase inhibitor) [10], tamoxifen (a selective oestrogen receptor modulator) [11] and staurosporine (a protein kinase inhibitor) [12] have been reported. Potential antibacterial ligands include quinolones which inhibit bacterial DNA gyrase and topoisomerase IV, enzymes that maintain the integrity of supercoiled DNA during DNA replication and transcription. However, their cross-reactivity with human class II topoisomerases has highlighted their potential as anti-cancer agents [13]. The crystal structure of a topoisomerase–DNA–quinolone (moxifloxacin) derivative provides evidence that the quinolone can bind the Mg^{2+} ion through *O,O′*-bidentate coordination with the remaining coordination sites occupied by aqua ligands which in turn form hydrogen bonds with DNA nucleobases [14]. Turel et al. have conjugated quinolones (ofloxacin [15], nalidixic acid [16] and cinoxacin [16]) to the Ru–arene framework with the Ru(II) π-bonded to a *p*-cymene (*p*-cym) ring and σ-bonded to the two oxygen atoms of the chelated quinolone with the remaining site occupied by a chloride ligand. All three complexes, upon hydrolysis, rapidly and selectively form adducts with guanosine 5′-monophosphate *via* coordination to *N*7, thus providing preliminary evidence that DNA may be a potential target. It has also been suggested that electrostatic interactions and hydrogen bonding may initially play a role in DNA recognition prior to guanosine 5′-monophosphate binding. Of the three complexes, only the ofloxacin derivative demonstrated *in vitro* cytotoxicity and in only one of the cell lines tested (CH1 with IC_{50} of 18 ± 7 μM) [16].

Fluoroquinolones are attractive for incorporation into metallodrugs with anti-bacterial properties since they possess a much broader spectrum of anti-bacterial activity as well as an enhanced pharmacokinetic profile when compared to quinolones. The antibiotic ciprofloxacin (Cip), a second generation orally or parentally administered fluoroquinolone, was the drug of choice to treat victims infected by anthrax in 2001 [17]. Structural optimisation of this lead drug molecule has led to derivatives with broad spectrum activities and minimal toxic side effects [18]. Metal complexes of Cip such as those of Co, Zn, Cd, Ni and Cu have also been investigated as an alternative strategy to optimise its therapeutic potential [19,20]. These complexes, in which Cip is bound *via O,O′*-bidentate coordination, have comparable anti-bacterial activity against several bacteria when compared to Cip itself. Interestingly, the complexes, in contrast to the ligand, are more bactericidal against stationary bacteria, a property which may be attractive for the treatment of chronic or device-related infections (*e.g.* catheter infections) which involve slowly metabolising bacteria in biofilm mode [21]. Vieira et al. recently reported a Pt–Cip derivative in which the antibiotic is complexed *via* piperazine *N,N′*-coordination. A positive correlation between lipophilicity, *in vitro* anti-tumour activity and rate of drug uptake was observed [22]. Furthermore, Azema et al. reported a structure activity study of 31 Cip derivatives investigating the correlation between lipophilicity and anti-tumour activity, with two lead candidates being identified, both demonstrating enhanced *in vitro* cytotoxicity in the low μM range against a panel of tumour cell lines as compared to the parent Cip [23]. Of the two, the 7-(4-(decanoyl)piperazin-1-yl) derivative CipA, Fig. 2, was most potent. These derivatives, particularly CipA, have IC_{50} values in the low μM range (3–7 μM in 4 cell lines tested), but were also non-toxic in an *in vivo* xenograft mouse model. While Cip is reported to have anti-proliferative and anti-cancer effects itself, harnessing its anti-bacterial activity in the cancer setting where significant infection risks are present due to immunosuppression, may augment its therapeutic effects. In the present work we attempt to combine into one drug molecule the anti-cancer properties of Ru–arene derivatives with the potent anti-bacterial and anti-cancer properties of CipA, with a view to generating novel multi-functional therapeutic agents to combat cancer.

Ruthenium(II) might bind to Cip ligands *via O,O′*- or *N,N′*-coordination. There is an example of a Ru(II)–piperazine complex in the literature with Ru(II) bound *via N,N′*-coordination, *i.e. trans*-dichloro-piperazine-*bis*(ether-phosphine)ruthenium(II) [24], and another, [(η^6-*p*-cym)$RuCl_2(CH_3NH(CH_2)_4NH)$]PF_6, in which the piperazine is bound *via* one nitrogen [25]. It therefore seemed possible that we could selectively and readily bind the 7-(4-(decanoyl)piperazin-1-yl) derivative of Cip to Ru(II) *via O,O′*-coordination given that *N*4 of the piperazine ring is no longer free to coordinate.

Our rationale was that the complex, upon tumour cell entry, might release CipA which can inhibit topoisomerases and/or bind DNA with the concomitant release of the Ru–arene framework free also to bind DNA. Release of chelating *O,O′*-ligands from Ru(II)–arene frameworks has been reported in the literature [26]. Herein, we report the synthesis and characterisation of CipA and Ru(η^6-*p*-cym)($CipA_{-H}$)Cl, including their X-ray crystal structures, as well as their anti-cancer and anti-bacterial properties.

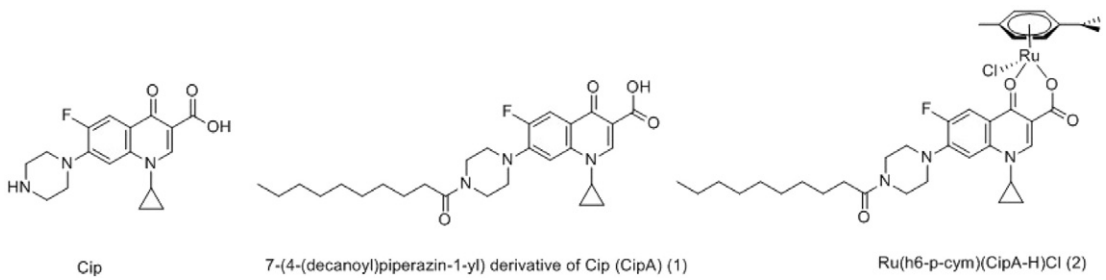

Fig. 2. Chemical structures of Cip, CipA (**1**) and [Ru(η^6-*p*-cym)($CipA_{-H}$)Cl] (**2**).

2. Materials and methods

All starting materials, including Cip (>98%) and [Ru(η^6-*p*-cym)Cl_2]$_2$ (>98%), were used as received from Sigma Aldrich. Propidium iodide (94%) and RNase were likewise purchased from Sigma Aldrich.

^{1}H, ^{13}C and ^{19}F NMR spectra were recorded using a Bruker DPX 400 spectrometer (at room temperature; 400 MHz, 101 MHz and 376 MHz, respectively). Coupling constants (*J*) are quoted in Hz. The splitting of the proton resonances is labelled as s = singlet, d = doublet, t = triplet, sept = septet, and m = multiplet. Chemical shifts (δ) are quoted in parts per million using residual protons in the indicated solvents as internal standards. All NMR data processing was carried out using MestReNova, version 6.0.2-5475. Infrared spectra were recorded on a Bruker Tensor 27 spectrometer with KBr as a standard. IR spectra were analysed using OPUS, version 5.0, with peak positions (ν) in cm^{-1}. Mass spectrometry was carried out with an Advion Expression Compact Mass Spectrometer: 10 μL of the samples was injected in 300 μL of methanol:water:formic acid (90:9:1 v/v). The mass spectrometry data were acquired both in positive and negative ion modes. Microanalyses were carried out at the Department of Chemistry, University College Dublin. Bacteria used for testing were *Escherichia coli* (*E. coli*) strain ATCC25922, an antibiotic susceptible laboratory strain and *E. coli* clinical isolate CL2, isolated from a patient with a urinary tract infection. CL2 is an extended spectrum β-lactamase (ESBL)-producer (resistant to 1st, 2nd and 3rd generation β-lactam antibiotics), belonging to the internationally disseminated pandemic clone 025b:H4-ST-131 *E. coli* [27].

2.1. Synthesis of CipA (**1**)

Cip (3 g, 9 mmol) and triethylamine (1.38 mL, 9.9 mmol) were stirred in dichloromethane (120 mL) at 273 K for 30 min. Decanoyl chloride (4.67 mL, 22.5 mmol) was added dropwise. After stirring at 273 K for an additional 45 min and then at room temperature for a further hour, water (100 mL) was added to the mixture. The aqueous layer was extracted with dichloromethane (2 × 50 mL). Combined organics were washed with water (20 mL) and dried over Na_2SO_4 and concentrated. The remaining residue was triturated in a copious amount of diethyl ether to generate an off-white solid, Fig. 3 (6.79 mmol, 75.4%). ^{1}H NMR (400 MHz, dmso-d_6): δ = 15.18 (s, 1H, –COO*H*), 8.67 (s, 1H, C*H* (6)), 7.93 (d, *J* = 13.2 Hz, 1H, C*H* (13)), 7.58 (d, *J* = 7.5 Hz, 1H, C*H* (10)), 3.86–3.77 (m, 1H, C*H* (7)), 3.71–3.62 (m, 4H, CH_2 (14, 16)), 3.40–3.25 (m, 4H, CH_2 (15, 17)), 2.36 (t, *J* = 7.5 Hz, 2H, CH_2 (19)), 1.59–1.45 (m, 2H, CH_2 (20)), 1.36–1.14 (m, 16H, CH_2 (8, 9, 21–26)), 0.85 (t, *J* = 6.8 Hz, 3H, CH_3). ^{13}C NMR (101 MHz, dmso-d_6): δ = 176.31 (*C*3), 170.80 (*C*18), 165.84 (*C*1), 154.14 (*C*12), 147.98 (*C*6), 144.89 (*C*11), 139.09 (*C*5), 118.74 (*C*4), 111.06 (*C*13), 110.83 (*C*2), 106.65 (*C*10), 49.69 (*C*14), 49.23 (*C*16), 44.56 (*C*15), 40.57 (*C*17), 35.84 (*C*7), 32.18 (*C*19), 31.26 (*C*20), 28.90 (*C*21–*C*23), 28.72 (*C*24), 24.74 (*C*25), 22.07 (*C*26), 13.91 (*C*27), 7.55 (*C*8, *C*9). ^{19}F NMR (376 MHz, dmso-d_6): δ = −121.77 (dd, *J* = 13.2, 7.5 Hz). ESI-MS (positive mode; MeOH) *m/z* 485.6 [M], 486.6 $[MH]^+$. IR selected bands (cm^{-1}, KBr): 2920, 1885, 1721, 1630, 1472, 1340, 1300, 1260, 1024, 949, 886 cm^{-1}. Anal. Calcd for $C_{27}H_{36}FN_3O_4$: C, 66.78; H, 7.47; N, 8.65; F, 3.91. Found: C, 66.70; H, 7.48; N, 8.70; F, 3.76.

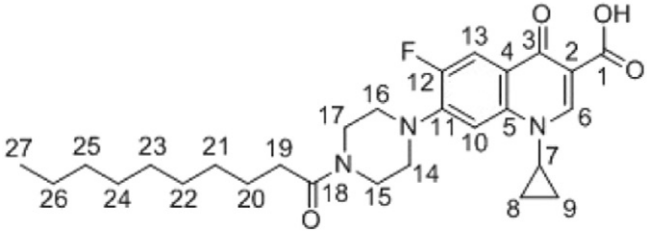

Fig. 3. Chemical structure of CipA (**1**).

2.2. Synthesis of [Ru(η^6-*p*-cym)(CipA$_{-H}$)Cl] (**2**)

CipA (0.13 mmol, 63.5 mg) was dissolved in chloroform/methanol (1/1) (20 mL). The mixture was left stirring at 333 K until all the CipA dissolved. Afterwards, NaOMe (0.13 mmol, 25% wt. in MeOH, 7.1 mg, 28 μL) was added dropwise. After an additional 15 min of stirring at room temperature, the solution was added dropwise to [Ru(η^6-*p*-cym)Cl_2]$_2$ (0.065 mmol, 40 mg) dissolved in chloroform/methanol (1/1) (50 mL) and the reaction mixture was refluxed for 48 h. The NaCl produced was removed by filtration through Celite. The solvent was removed *in vacuo*. A few drops of dichloromethane and *n*-hexane (15 mL) were added to the light orange waxy residue to give a light yellow solid. The solid was filtered off and dried under vacuum to afford a yellow flaky solid (0.072 mmol, 55.4%). ^{1}H NMR (400 MHz, dmso-d_6): δ = 8.59 (s, 1H, C*H* (6)), 8.03 (d, *J* = 13.5 Hz, 1H, C*H* (13)), 7.48 (d, *J* = 7.5 Hz, 1H, C*H* (10)), 5.74 (t, *J* = 6.6 Hz, 2H, Ar-*H* cym), 5.43 (t, *J* = 6.6 Hz, 2H, Ar-*H* cym), 3.74–3.67 (m, 5H, C*H* (7), CH_2 (14, 16)), 3.25 (s, 4H, CH_2 (15, 17)), 2.90 (sept, 1H, Ar-C*H*$(CH_3)_2$ cym), 2.35 (t, *J* = 7.3 Hz, 2H, CH_2 (19)), 2.17 (s, 3H, Ar-CH_3 cym), 1.51 (s, 2H, CH_2 (20)), 1.31 (d, *J* = 6.9 Hz, 6H, Ar-CH(CH_3)$_2$), 1.27–1.01 (m, 16H, CH_2 (8, 9, 21–26)), 0.85 (t, *J* = 6.4 Hz, 3H, CH_3 (27)). ^{13}C NMR (101 MHz, dmso-d_6): δ = 170.79 (*C*3, *C*18), 165.39 (*C*1), 151.82 (*C*12), 148.45 (*C*6), 144.50 (*C*11), 137.28 (*C*5), 119.53 (*C*4), 112.42 (*C*13), 111.72–110.87 (*C*2, *C*10), 97.99 (Ar-*C* cym), 96.15 (Ar-*C* cym), 82.34 (Ar-*C*H cym), 82.05 (Ar-*C*H cym), 77.95 (Ar-*C*H cym), 77.82 (Ar-*C*H cym), 49.81 (*C*14), 49.30 (*C*16), 44.57 (*C*15), 40.56 (*C*17), 35.51 (*C*7), 32.18 (*C*19), 31.26 (*C*20), 30.40 (Ar-*C*H$(CH_3)_2$), 28.90 (*C*21–*C*23), 28.72 (*C*24), 24.76 (*C*25), 22.03 (*C*26, Ar-CH(*C*H$_3$)$_2$), 17.58 (Ar-*C*H$_3$), 13.93 (*C*27), 7.54 (*C*8, *C*9). ^{19}F NMR (376 MHz, dmso-d_6): δ = −122.21 (dd, *J* = 13.5, 7.4 Hz). ESI-MS (positive mode; MeOH) *m/z* 755.2 [M], 719.91 $[M-Cl]^+$. IR selected bands (cm^{-}1, KBr): 2925, 1651, 1631, 1552, 1519, 1481, 1298, 1261, 1021, 949, 885 cm^{-1}. Anal. Calcd for $C_{37}H_{49}ClFN_3O_4Ru.0.5H_2O$: C, 58.14; H, 6.59; N, 5.34; Cl, 4.64; F, 2.49. Found: C, 57.96; H, 6.13; N, 5.37; Cl, 4.37; F, 2.24.

2.3. Structure analysis

Crystallographic data for CipA and [Ru(η^6-*p*-cym)(CipA$_{-H}$)Cl] were collected on a Bruker APEX DUO with Mo Kα radiation (λ = 1.54178 and 0.71073 Å) using a MiTeGen micromount and at 100(2) K (Oxford Cobra Cryosystem). Bruker APEX2 [28] software was used to collect and reduce data, determine the space group, solve and refine the structure. Absorption corrections were applied using SADABS [29]. Final

Table 1
Crystal data and structure refinement for **1**·1.3H_2O·0.6CH_3OH and **2**·CH_3OH·0.5H_2O.

	1	**2**
Empirical formula	$C_{27.60}H_{41}FN_3O_{5.90}$	$C_{76}H_{108}Cl_2F_2N_6O_{11}Ru_2$
fw	528.23	1592.72
Crystal system	Triclinic	Triclinic
Space group	Pī	Pī
a (Å)	8.1142(4)	8.6844(4)
b (Å)	9.6285(4)	9.3426(4)
c (Å)	17.8315(8)	23.7743(12)
β (°)	100.003(2)	92.3359(15)
V (Å^3)	90.839(2)	99.2449(15)
T (K)	96.521(3)	91.4334(15)
Z	2	1
ρ (mg/cm^3)	1.288	1.391
μ (mm^{-1})	0.781	0.534
Total reflns	35,732	74,715
Indep. reflns	4937	11,051
R(int)	0.0869	0.0572
S	1.038	1.097
R_1[a] [I > 2σ(I)]	0.0591	0.045
wR_2 [I > 2σ(I)]	0.1573	0.0931
CCDC number	1429461	1429462

[a] $R_1 = \Sigma||F_o| - |F_c||/\Sigma|F_o|$, $wR_2 = [\Sigma w(F_o^2 - F_c^2)^2/\Sigma w(F_o^2)^2]^{1/2}$.

refinements were performed with SHELXL [30]. All non-hydrogen atoms were refined anisotropically. For refinement details see supplementary crystallographic data. See Table 1 for crystal data and structure refinement parameters. CCDC 1429461 and 1429462 contain the supplementary crystallographic data for this paper.

2.4. Cell culture

A2780, A549, HCT116, and PC3 cells of ovarian, lung, colon and prostate origin, together with their derived cell lines A2780Cis (cisplatin (CDDP) resistant), HCT116Ox (oxaliplatin (OXA) resistant) and HCT116p53 (p53 knocked out) were obtained from the European Collection of Cell Cultures (ECACC) and grown in Roswell Park Memorial Institute medium (RPMI-1640), Dulbecco's modified Eagle's medium, or McCoy's Modified 5A medium supplemented with 10% v/v of foetal calf serum, 1% v/v of 2 mM glutamine and 1% v/v penicillin/streptomycin. All cells were grown as adherent monolayers at 310 K in a 5% CO_2 humidified atmosphere and passaged at approximately 70–80% confluency.

2.5. In vitro growth inhibition assay

Briefly, 96-well plates were used to seed 5000 cells per well. The plates were left to pre-incubate in drug-free medium at 310 K for 48 h before adding different concentrations of the compounds to be tested. A drug exposure period of 24 h was allowed. After this, supernatants were removed by suction and each well was washed with phosphate-buffered saline (PBS). A further 72 h was allowed for the cells to recover in drug-free medium at 310 K. The sulforhodamine B (SRB) assay was used to determine cell viability [31]. IC_{50} values, as the concentration which caused 50% of cell death, were determined as duplicates of triplicate in two independent sets of experiments and their standard deviations were calculated. Cells exposed to cisplatin or oxaliplatin as well as untreated cells were used as positive and negative controls respectively.

2.6. Cell cycle analysis

A549 lung cancer cells were seeded in a 6-well plate using 1.0×10^6 cells per well. They were pre-incubated in drug-free medium at 310 K for 24 h, after which [Ru(η^6-*p*-cym)(CipA$_{-H}$)Cl] was added using equipotent concentrations equal to IC_{50} and $2\times$ IC_{50}. After 24 h of drug exposure, supernatants were removed by suction and cells were washed with PBS. Finally, cells were harvested using trypsin. DNA staining was achieved by re-suspending the cell pellets in PBS containing propidium iodide and RNAse A. Cell pellets were re-suspended in PBS before being analysed by flow cytometry using the maximum excitation of propidium iodide-bound DNA at 536 nm, and its emission at 617 nm. Data were processed using Flowjo software. These experiments used untreated cells as negative controls, and cisplatin-exposed cells as positive controls. All experiments were carried out in triplicate. Although only selected histograms are shown, full numerical data and statistical analysis can be found in the Supporting Information.

2.7. Induction of apoptosis

Flow cytometry analysis of apoptotic populations was carried out using the Annexin V-FITC Apoptosis Detection Kit (Sigma Aldrich) according to the manufacturer's instructions. Briefly, A549 lung cancer cells were seeded in 6-well plates (1.0×10^6 cells per well), pre-incubated for 24 h in drug-free media at 310 K, after which they were exposed to [Ru(η^6-*p*-cym)(CipA$_{-H}$)Cl] for a further 24 h (equipotent concentrations equal to IC_{50} and $2\times$ IC_{50}). Cells were harvested using trypsin and stained using propidium iodide/Annexin V-FITC. After staining in the dark, cell pellets were analysed in a Becton Dickinson FACScan Flow Cytometer. For positive-apoptosis controls A549 cells were exposed for 2 h to staurosporine (1 μg/mL) or for 24 h to cisplatin. Cells for apoptosis studies were used with no previous fixing procedure as to avoid non-specific binding of the Annexin V-FITC conjugate. Negative controls included untreated cells. These experiments were carried out in triplicate, although only selected dot plots are shown, full numerical data and statistical analysis can be found in the Supporting Information.

2.8. Statistical analysis

In all cases, independent two-sample t-tests with unequal variances, Welch's tests, were carried out to establish statistical significance of the variations ($p < 0.01$ for **, and $p < 0.05$ for *).

2.9. Bactericidal assays

A modification of a previously described method was used [32]. Briefly, bacteria were grown overnight at 310 K on Mueller-Hinton (MH) agar. Suspensions were prepared from isolated colonies to the density of a 0.5 McFarland standard (bioMérieux, Ireland) using a densitometer (Densichek, bioMérieux). The suspension was further diluted 1/10 in MH broth. Tested agents were dissolved in 10% DMSO in 10 mM potassium phosphate buffer (pH 6.8). Assays of 100 μL volumes were prepared in microcentrifuge tubes and contained 0 to 500 μM tested agents, 10% (vol/vol) *E. coli* (ca. $1.5–10^5$ CFU/mL), and 10 mM potassium phosphate buffer, pH 6.8. Assay mixtures were incubated at 310 K and 120 rpm in a shaking incubator (Gallenkamp, United Kingdom) for 1 h and then diluted 1/10 with 0.95% (wt/vol) NaCl. After vortex-mixing for 30 s, 10–100 μL aliquots were spread onto MH agar and incubated overnight at 310 K. Percentage killing activity was calculated from viable counts (CFU/mL) from assays containing tested agents compared to control assays not containing tested agents.

3. Results and discussion

The synthesis of CipA was carried out following a previously reported procedure with one slight modification [23]. Treatment of commercially available Cip with decanoyl chloride in the presence of triethylamine generated a white solid in good yield and excellent purity. In contrast with the reported method where silica gel chromatography (eluent: CH_2Cl_2–MeOH 1–2%) was used to achieve the desired purity of CipA, trituration with diethyl ether served this purpose based on differences in solubilities between CipA and unreacted starting materials. Suitable crystals of CipA for X-ray diffraction analysis were obtained from a methanol solution upon slow evaporation at room temperature.

Treatment of [Ru(η^6-*p*-cym)Cl$_2$]$_2$ with CipA in the presence of sodium methoxide afforded [Ru(η^6-*p*-cym)(CipA$_{-H}$)Cl] in good yield and excellent purity. [Ru(η^6-*p*-cym)(CipA$_{-H}$)Cl] was isolated as a yellow flaky solid which was both air and moisture stable. Needle-like light orange crystals of [Ru(η^6-*p*-cym)(CipA$_{-H}$)Cl]·CH_3OH·$0.5H_2O$, suitable for X-ray analysis, were obtained by slow evaporation of a dichloromethane and *n*-hexane mixture. To assess the likelihood of intracellular CipA release, the stability of complex **2** under aqueous conditions was monitored by ^{1}H NMR spectroscopy, the details of which are provided in Supporting Information. The release of CipA from **2** was observed in under an hour.

3.1. Solid state structures

The complex [Ru(η^6-*p*-cym)(CipA$_{-H}$)Cl], Fig. 4 adopts a typical pseudo-octahedral 'piano-stool' geometry, with Ru(II) π-bonded to the *p*-cymene ring and σ-bonded to a chloride and two oxygen atoms of the chelated fluoroquinolone ligand. When comparing the crystal structure of CipA, Fig. 4 to that of the complex, we can see a slight lengthening of the d(C1–O2) carbonyl bond from 1.213(3) to 1.243(3) Å, indicative of delocalisation, Table 2. The expected shortening of the bond between d(C1–O1) in [Ru(η^6-*p*-cym)(CipA$_{-H}$)Cl] is also observed. The distances between Ru(II) and the exocyclic carbonyl

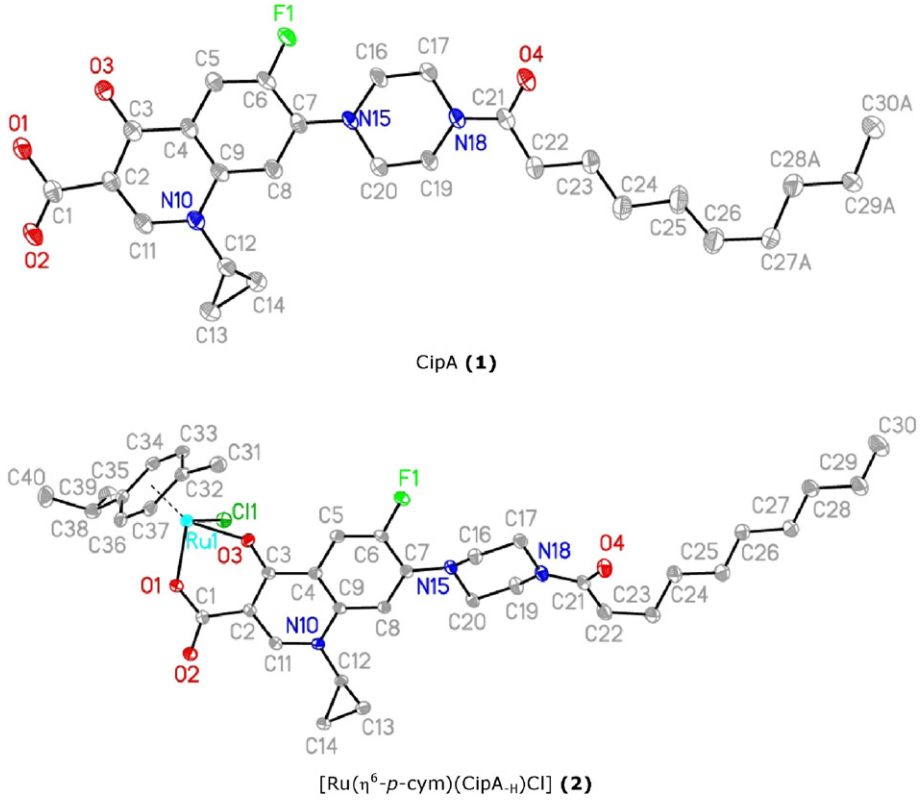

Fig. 4. (Top) Molecular structure of **1** with atomic displacement parameters shown at 50% probability. Only one conformation of the disordered chain is shown for clarity. Hydrogen atoms and solvent molecules (1.3 H_2O in two positions and 0.6 CH_3OH) omitted for clarity also. (Bottom) Molecular structure of **2** with atomic displacement parameters shown at 50% probability. Hydrogen atoms and disordered solvent (CH_3OH in two positions; 0.5 H_2O) omitted for clarity.

and carboxylate oxygens are 2.0897(17) Å and 2.0875(17) Å, respectively, consistent with literature reports. The Ru–Cl bond length is 2.4214(6) Å, within the expected range. The metal to ring centroid distance d(Ru1–cymene$_{centroid}$) is 1.6396(2) Å, again consistent with literature reports. The O1–Ru–O3 and O–Ru–Cl angles are between 83.53° and 86.76°. This is within the same range as previously reported for other similar Ru–cymene complexes [33]. CipA co-crystallised with a water/methanol mixture (one fully occupied water molecule and partially occupied water and methanol molecules). The water forms strong hydrogen bonds with the carbonyl oxygens (d(O3–O$_{water}$), d(O4–O$_{water}$) of 2.863(3) and 2.721(2) Å respectively). On the other hand, [Ru(η^6-*p*-cym)(CipA$_{-H}$)Cl] co-crystallised with a mixture of water and methanol (one molecule of methanol disordered over two positions and a half occupied water molecule), despite the complex being recrystallised from a mixture of dichloromethane:hexane. The molecule of water forms hydrogen bonds with the chloride on Ru(II) (d(Cl–O$_{water}$) of 3.310(4) Å) and the carbonyl oxygen (d(O2–O$_{water}$) of 2.715(4) Å). One molecule of methanol forms a hydrogen bond with the chloride (d(Cl–O$_{methanol}$) of 3.211(4) Å) and the other molecule of methanol hydrogen bonds with the uncoordinated decanoyl carbonyl oxygen (d(O4–C$_{methanol}$) of 2.927(7) Å).

Table 2
Selected bond lengths and angles for **1**·1.3H_2O·0.6CH_3OH and **2**·CH_3OH·0.5H_2O.

		1	2
Bond lengths/Å	C1–O1	1.337(3)	1.279(3)
	C1–O2	1.213(3)	1.243(3)
	C3–O3	1.274(2)	1.279(3)
	Ru–O1	–	2.0875(17)
	Ru–O3	–	2.0897(17)
	Ru–Cl	–	2.4214(6)
	Ru–cymene$_{centroid}$	–	1.6396(2)
Angle/°	O1–Ru–O3	–	86.10(7)
	O1–Ru–Cl	–	86.76(5)
	O3–Ru–Cl	–	83.53(3)

3.2. Anti-proliferative activity

The anti-proliferative activity of Cip, CipA and [Ru(η^6-*p*-cym)(CipA$_{-H}$)Cl] towards a variety of human cancer cell lines of ovarian, lung, prostate and colon origin was investigated and compared to that of cisplatin and oxaliplatin which were used as positive controls, Table 3. Interestingly, in all cases [Ru(η^6-*p*-cym)(CipA$_{-H}$)Cl] resulted in significantly enhanced cytotoxicity as compared to its organic chelating ligand, CipA and the corresponding biologically active precursor, Cip. The metal complex [Ru(η^6-*p*-cym)(CipA$_{-H}$)Cl] was highly cytotoxic in all cell lines tested with potencies in the low μM range (0.25 to 6.2 μM), comparable to the activity of cisplatin. The chelating ligand CipA, in contrast, was cytotoxic in A2780 ovarian, A549 lung and PC3 prostate cancer lines, but to a much lesser extent with values ranging between 7 and 15 μM. Cip was inactive in all cell lines tested.

In the A2780 human ovarian cell line, there is an order of magnitude difference in potency between CipA and [Ru(η^6-*p*-cym)(CipA$_{-H}$)Cl]. Interestingly, the ligand CipA loses activity in the cisplatin-resistant cell line A2780Cis with an IC_{50} value >50 μM, in stark contrast to the Ru complex which shows a resistance factor of only 1.65 (calculated as the ratio between the IC_{50} values in the resistant and IC_{50} in the parental line). It has been proposed that the underlying resistance associated with A2780Cis involves a two-fold more efficient efflux and a consequent reduction in cellular accumulation as compared to the parental A2780 as well as an increase in DNA-repair mechanisms [34]. The mechanism of action of [Ru(η^6-*p*-cym)(CipA$_{-H}$)Cl] must therefore differ from cisplatin given that it demonstrates low μM cytotoxicity in both the cisplatin-sensitive and -resistant A2780 cell lines. Another striking result is observed for the HCT116 colon cancer cell line. Cip and CipA are inactive, with IC_{50} values >100 μM, while [Ru(η^6-*p*-cym)(CipA$_{-H}$)Cl]

Table 3
Cytotoxicities of Cip, CipA (**1**), [Ru(η⁶-*p*-cym)(CipA_H)Cl] (**2**), cisplatin (CDDP) and oxaliplatin (OXA) against A2780, A2780Cis, A549, HCT116, HCT116Ox, HCT116p53 and PC3 cell lines.

Compound	IC_{50}/μM						
	A2780	A2780Cis	A549	HCT116	HCT116Ox	HCT116p53	PC3
Cip	>50	>75	>50	>100	>100	>100	>50
1	11.2 ± 0.4	>50	7.0 ± 0.3	>100	>100	>100	15.6 ± 0.3
2	1.027 ± 0.004	1.7 ± 0.1	0.25 ± 0.04	1.33 ± 0.07	1.93 ± 0.03	6.2 ± 0.8	1.46 ± 0.08
CDDP	1.2 ± 0.2	11.5 ± 0.3	3.3 ± 0.1	5.1 ± 0.3	N/D	36.7 ± 0.3	N/D
OXA	N/D	N/D	N/D	3.99 ± 0.08	32.2 ± 0.5	>100	N/D

has an IC_{50} of 1.33 ± 0.07 μM in the parental cell line and 1.93 ± 0.03 μM in the oxaliplatin-resistant derived line HCT116Ox (resistant factor = 1.45). Oxaliplatin resistance associated with HCT116Ox has been linked to apoptosis regulator BAX expression resulting in an increase in gluthathione-S-transferase levels; this increase facilitates cellular detoxification and reduction in levels of Pt–DNA adducts as a consequence of an increase in DNA repair [35]. Again, the mechanism of action of [Ru(η⁶-*p*-cym)(CipA_H)Cl] must therefore differ from oxaliplatin given that it demonstrates low μM cytotoxicity in both the oxaliplatin-sensitive and -resistant HCT116 cell lines. Given that [Ru(η⁶-*p*-cym)(CipA_H)Cl] has been shown to be highly cytotoxic against these two resistant cell lines would therefore suggest that cellular processes such as reduced accumulation, increased efflux or enhanced DNA repair mechanisms, all of which have been implicated in the resistance associated with cisplatin and oxaliplatin, do not appear to affect the anti-proliferative activity of [Ru(η⁶-*p*-cym)(CipA_H)Cl].

In order to further elucidate the mechanism of action of [Ru(η⁶-*p*-cym)(CipA_H)Cl], we sought to investigate the involvement of oncogene p53 in its activity. Tumour suppressor p53, known as the guardian of the genome, is involved in facilitating DNA repair before DNA replication [36,37]. Modifications in its expression before or after chemotherapy can lead to transcriptional activation of p21 and p73 which results in apoptosis. Most importantly, there is a close connection between cell cycle arrest and the expression of this tumour suppressor. This is particularly true in colorectal cancers in which p53 is found to be mutated in more than 50% of clinical cases and the status of p53 can influence directly the sensitivity to the Pt drugs, cisplatin and especially oxaliplatin. Inactive p53 oncogene has been linked to poor patient prognosis and treatment failure [38]. We therefore investigated the involvement of oncogene p53 in the activity of [Ru(η⁶-*p*-cym)(CipA_H)Cl] in the colorectal cell line HCT116 and compared it to that of oxaliplatin. For this we determined the anti-proliferative activity of tested compounds in a derived cell line which had the tumour suppressor p53 knocked out. Our data show that [Ru(η⁶-*p*-cym)(CipA_H)Cl] retains activity in the HCT116p53 mutated cell line with an IC_{50} value of 6.2 ± 0.8 μM (resistance factor of 4.6) when compared to oxaliplatin (resistant factor > 25). This suggests that the status of p53 is not highly relevant for the anti-cancer activity of [Ru(η⁶-*p*-cym)(CipA_H)Cl] and that the mechanism of action of this novel drug may not involve the activation of this oncogene.

3.3. Flow cytometry

Based on the anti-proliferative activity results, further analysis of the cellular behaviour of [Ru(η⁶-*p*-cym)(CipA_H)Cl] was performed in the A549 lung cancer cell line, where it showed sub-μM potency. Its effect on the cell cycle profile of cells exposed to equipotent concentrations of [Ru(η⁶-*p*-cym)(CipA_H)Cl] equal to 1× and 2× the IC_{50} values was investigated. The induction of apoptosis under similar conditions was also investigated. In both cases, the data for [Ru(η⁶-*p*-cym)(CipA_H)Cl] were compared to the results obtained when the same cell line was exposed to cisplatin at IC_{50} concentrations.

Cell cycle profiles can be readily obtained by flow cytometry using propidium iodide staining, as it binds quantitatively to nuclear DNA of fixed cells. Fluorescence measured in the FL2 red channel can be related to the number of DNA copies present in the single cell suspension analysed, so populations in the G1, G2/M and S phases can be quantified. Two concentrations of [Ru(η⁶-*p*-cym)(CipA_H)Cl] were used and the populations in the three cell cycle phases to those of an untreated negative control and a cisplatin-exposed positive control were compared, Fig. 5. As expected, the negative controls showed most of the population in a G1 phase (72.6%) with similar values for the S and G2/M phases (13.7 and 13.5% respectively). In comparison, cisplatin-exposed cells show a sharp increase in the S phase population (up to 29.5%) while the G1 decreases to 54% and the G2/M remains approximately stable at 14.8%. This clear S-phase arrest caused by the platinum-based drug is very well established in the literature and it is a consequence of a mechanism of action that involves coordinative binding to the double helix and subsequent structural modification of the cellular DNA [39,40].

Cells treated with [Ru(η⁶-*p*-cym)(CipA_H)Cl] showed a statistically significant change in the population distribution, with the G1 phase reducing to 59 and 56% when exposed to 1× and 2× IC_{50} concentrations, respectively, Fig. 5 and Supporting Information. In consequence, the S and G2/M phases increase. It is however not possible to establish if there is a significant arrest in any of these two particular phases as the

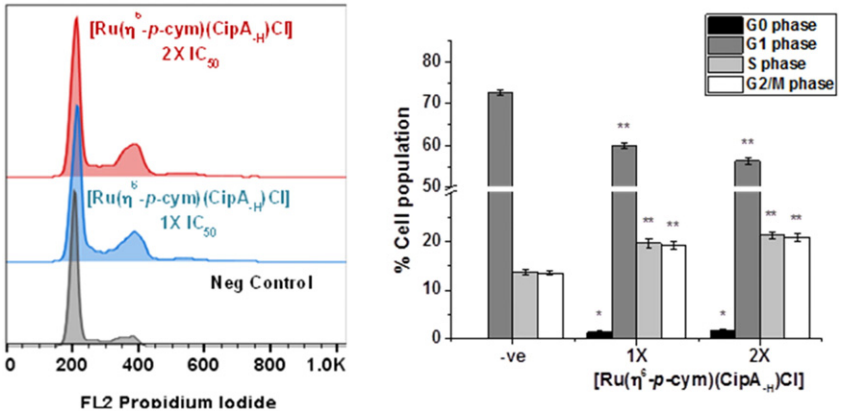

Fig. 5. Cell cycle analysis of A549 cells exposed to [Ru(η⁶-*p*-cym)(CipA_H)Cl at equipotent concentrations equal to 1× and 2× IC_{50}. Left: Flow cytometry histograms of the FL2 red channel reading propidium iodide fluorescence. Right: bar chart showing the percentage cell population present in each of the cell cycle phases, ($p < 0.01$ for **, and $p < 0.05$ for *).

population percentages in both remain approximately the same even at the highest concentration (21 and 20% for S and G2/M phases, respectively). It is also possible that the mechanism of action of [Ru(η^6-*p*-cym)(CipA$_{-H}$)Cl] involves DNA interaction and a subsequent S phase arrest, as well as a disruption of the mitotic machinery which could lead to a G2/M arrest. Importantly, this S/G2/M arrest has also been observed previously in transitional bladder cell carcinoma (HTB9 cell line) treated with Cip, possibly due to modulation of key cell cycle regulatory genes and the downregulation of initial trigger for antigen-presenting cell activation in mitosis, Cyclin B/cdc2-kinase, which is also necessary for degradation of mitotic cyclins [41].

Apoptosis, programmed cell death, is a cellular process often involved in the anti-proliferative activity of metal-based complexes. Its induction after drug exposure can be followed by flow cytometry analysis using a combination of Annexin V and propidium iodide staining. Viable cells should exhibit low fluorescence when observed in a FL1-green and FL2-red dot plot, while early apoptotic cells should be located in a quadrant with high Annexin V and low propidium iodide fluorescence. In this case, cells have lost the symmetry of the phospholipid membrane and allow Annexin binding only. In late stages of apoptosis, the integrity of the membrane is lost and cells become permeant to the nuclear intercalator, which would locate them in a flow cytometry quadrant with high Annexin and high propidium iodide fluorescence. The last quadrant, which corresponds to low Annexin V but high propidium iodide fluorescence, shows non-viable cells.

Untreated controls used as comparison, as expected, showed the majority of the population in the quadrant with low fluorescence for both stains. Meanwhile cells exposed to cisplatin, used as a positive control, showed a statistically significant increase in the population of non-viable cells (high propidium iodide) and late apoptotic cells (high fluorescence reading in both channels), Fig. 6 and Supporting Information.

Cells exposed to [Ru(η^6-*p*-cym)(CipA$_{-H}$)Cl], in contrast, had a statistically relevant increase of cells in the three quadrants that have high fluorescence, particularly in those that have high readings for propidium iodide as a nuclear staining, Fig. 6. At the highest concentration tested, the population of viable cells (low Annexin V, low propidium iodide) varied from 97 to 81% while the late apoptotic population (high Annexin V, high propidium iodide) increased from 0.4 to 6.5%. Interestingly, the population that showed only high propidium iodide fluorescence increased from 0.5 to 7%, Fig. 6. These studies indicate that [Ru(η^6-*p*-cym)(CipA$_{-H}$)Cl] begins to induce apoptosis after 24 h of drug exposure, but most importantly that this may not be the only cell death process occurring. As mentioned before, the anti-cancer activity of Cip has been investigated against HTB9 bladder carcinoma cells. In this case, Cip induces significant apoptosis but only after 72 h of drug exposure. At this point there is proteolytic cleavage of poly (ADP-ribose) polymerase (proteins involved in a number of cellular processes including programmed cell death and DNA repair) and a significant alteration of the ratio between BAX and one of the proteins that regulates cell death, Bcl-2. At 24 h of drug exposure, it seems that BAX could be translocated into the mitochondria, but its concentration is not high enough to induce mitochondrial membrane potential changes and activation of the caspase cascade which will in turn result in apoptosis [41]. The slow induction of apoptosis observed does not rule out the involvement of parallel mechanisms of cell death, in fact, metal-based complexes are often multi-targeted and can have multiple mechanisms of action [42,43].

Cip has also been investigated for the treatment of pancreatic cancers. Here, the fluoroquinolone induces apoptosis after triggering both intrinsic and extrinsic pathways with activation of caspases 8, 9, and 3 (some of the cysteine proteases that play essential roles in apoptosis). It has even been suggested that pathways such as the extracellular signal-regulated kinase (ERK) pathway could be involved in its mechanism of action. Interestingly, it is also known that cisplatin induces apoptosis after activation of this pathway. Saini et al. studied the combination of Cip and cisplatin as a 48 h co-administration. They attributed the observed increase in the anti-proliferative activity to the double activation of ERK1/2 [44]. In light of the above, further studies will be required to understand more fully the mechanism of action of [Ru(η^6-*p*-cym)(CipA$_{-H}$)Cl].

Table 4
Bactericidal activity of test agents against *E. coli.*

Compound	% bactericidal activity*	
	E. coli	ESBL-*E. coli*
	Strain ATCC25922	CL2
Cip	83.4 ± 9.9[a]	91.7 ± 2.9[a]
	84.4 ± 8.0[b]	94.4 ± 2.3[b]
	99.4 ± 0.4[c]	94.4 ± 1.7[c]
1	98.5 ± 0.8[a]	72.8 ± 15.9[a]
	99.7 ± 0.1[b]	75.0 ± 14.8[b]
	99.6 ± 0.3[c]	80.0 ± 11.0[c]
2	38.9 ± 12.9[a]	19.9 ± 7.0[a]
	51.2 ± 12.2[b]	30.3 ± 4.0[b]
	48.9 ± 12.9[c]	52.1 ± 7.4[c]

*Data represent mean ± SEM of the results of 3 separate determinations carried out in duplicate over the concentration range ([a] — 200 μM, [b] — 400 μM, [c] — 500 μM). A fixed number of bacteria (1×10^5 CFU/mL) were exposed to the agent for 1 h and % killing was calculated compared to controls which were not exposed to the agent.

3.4. Bactericidal activity

The bactericidal activity of Cip, CipA and [Ru(η^6-*p*-cym)(CipA$_{-H}$)Cl] is summarised in Table 4. The Ru–cymene starting material, [Ru(η^6-*p*-cym)Cl$_2$]$_2$, showed no activity against *E. coli* over the concentration

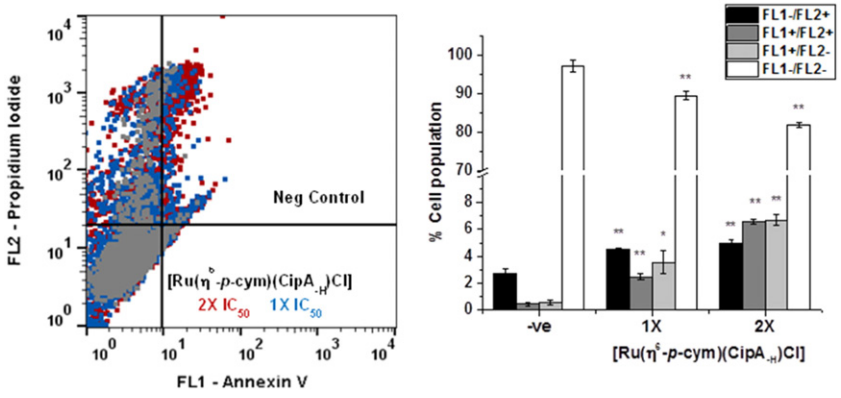

Fig. 6. Induction of apoptosis of A549 cells exposed to [Ru(η^6-*p*-cym)(CipA$_{-H}$)Cl] at equipotent concentrations equal to 1× and 2× IC_{50}. Left: Flow cytometry dot plot showing FL1 Green Annexin V fluorescence and FL2 red propidium iodide fluorescence. Right: bar chart showing the percentage cell population present in each of the dot plot quadrants, ($p < 0.01$ for **, and $p < 0.05$ for *).

range tested (50–500 μM, data not shown). Cip and CipA demonstrated killing activity in the range 72.8–99.7% against antibiotic susceptible and ESBL-*E. coli* over the concentration range 50–500 μM. [Ru(η^6-*p*-cym)(CipA$_{-H}$)Cl] had moderate activity against both strains of *E. coli* which appeared dose dependent for ESBL-*E. coli*. The highest extent of killing by the complex was 49% and 52% for fully susceptible *E. coli* and ESBL-*E. coli*, respectively (at 500 μM; 1 h incubation). The reduced potency observed compared to CipA may reflect reduced uptake of the complex across the Gram-negative cell envelope or inefficient release of CipA from the complex when internalised. However, these data indicate that up to half of the potency of Cip is retained when complexed to Ru, at least under the conditions tested. The retention of this property when combined with its potent cytotoxic effects in three cancer cell lines is encouraging and can form the basis for further investigation of its anti-bacterial activity particularly in the context of cancer. Such studies might involve particularly antibiotic-resistant strains that are clinically significant in the context of cancer and cause healthcare-associated infections in the immunocompromised including central venous or peripheral line infections. It should be noted however that the concentrations of [Ru(η^6-*p*-cym)(CipA$_{-H}$)Cl] at which *in vitro* bactericidal activity was observed are an order of magnitude greater than the concentration range at which anti-proliferative activity was found. Further investigation of the bactericidal activity under assay conditions that more closely mimic the *in vivo* environment of infection, may reduce this differential.

4. Conclusion

A half-sandwich, 'piano-stool' organo-ruthenium(II) arene complex [Ru(η^6-*p*-cym)(CipA$_{-H}$)Cl] which incorporates 7-(4-(decanoyl)piperazin-1-yl)-ciprofloxacin as an *O,O′*-chelated ligand has been synthesised, and the x-ray crystal structures of both the complex and the ciprofloxacin analogue have been determined. The complex is highly cytotoxic in the low μM range and is as potent as the clinical drug cisplatin against the human cancer cell lines A2780, A549, HCT116, and PC3 of ovarian, lung, colon and prostate origin, as well as cisplatin- and oxaliplatin-resistant cell lines suggesting a different mechanism of action. The complex also retained low μM cytotoxicity against the human colon cancer cell line HCT116p53 in which the tumour suppressor p53 had been knocked out, suggesting that the potent anti-proliferative properties associated with this complex are independent of the status of p53 (in contrast to cisplatin). The complex also retained moderate and dose-dependent anti-bacterial activity in both *E. coli*, one of which was a clinical isolate resistant to first, second and third generation β-lactam antibiotics. In conclusion, we have successfully employed a multi-functional approach to combine into one drug molecule the anti-cancer properties of Ru(II)–arene derivatives with the anti-cancer and anti-bacterial properties of CipA.

Acknowledgements

We thank the Science Foundation Ireland (Grant Nos. 11/RFP.1/CHS/3095 and 12/TIDA/B2384), the ERC (Grant No. 247450) and EPSRC (Grant No. EP/F042159/1) for their support for this work. We thank Professor Iztok Turel (University of Ljubljana, Slovenia) for the helpful discussions and also acknowledge COST CM1105 for being a platform to progress fruitful collaborations and for funding two highly valuable short-term scientific missions for ZU to conduct research in the laboratory of PJS.

Appendix A. Supplementary data

Supplementary data to this article can be found online at http://dx.doi.org/10.1016/j.jinorgbio.2016.02.018.

References

[1] J.P. Parker, Z. Ude, C.J. Marmion, Metallomics 8 (2016) 43–60.
[2] J.M. Rademaker-Lakhai, D. van den Bongard, D. Pluim, J.H. Beijnen, J.H. Schellens, Clin. Cancer Res. 10 (2004) 3717–3727.
[3] S. Leijen, S.A. Burgers, P. Baas, D. Pluim, M. Tibben, E. van Werkhoven, E. Alessio, G. Sava, J.H. Beijnen, J.H. Schellens, Investig. New Drugs 33 (2015) 201–214.
[4] P.S. Kuhn, V. Pichler, A. Roller, M. Hejl, M.A. Jakupec, W. Kandioller, B.K. Keppler, Dalton Trans. 44 (2015) 659–668.
[5] C.G. Hartinger, M.A. Jakupec, S. Zorbas-Seifried, M. Groessl, A. Egger, W. Berger, H. Zorbas, P.J. Dyson, B.K. Keppler, Chem. Biodivers. 5 (2008) 2140–2155.
[6] C.G. Hartinger, S. Zorbas-Seifried, M.A. Jakupec, B. Kynast, H. Zorbas, B.K. Keppler, J. Inorg. Biochem. 100 (2006) 891–904.
[7] R.E. Morris, R.E. Aird, S. Murdoch Pdel, H. Chen, J. Cummings, N.D. Hughes, S. Parsons, A. Parkin, G. Boyd, D.I. Jodrell, P.J. Sadler, J. Med. Chem. 44 (2001) 3616–3621.
[8] R.E. Aird, J. Cummings, A.A. Ritchie, M. Muir, R.E. Morris, H. Chen, P.J. Sadler, D.I. Jodrell, Br. J. Cancer 86 (2002) 1652–1657.
[9] Z. Adhireksan, G.E. Davey, P. Campomanes, M. Groessl, C.M. Clavel, H. Yu, A.A. Nazarov, C.H. Yeo, W.H. Ang, P. Droge, U. Rothlisberger, P.J. Dyson, C.A. Davey, Nat. Commun. 5 (2014) 3462.
[10] W.H. Ang, A. De Luca, C. Chapuis-Bernasconi, L. Juillerat-Jeanneret, M. Lo Bello, P.J. Dyson, ChemMedChem 2 (2007) 1799–1806.
[11] A. Vessieres, S. Top, W. Beck, E. Hillard, G. Jaouen, Dalton Trans. (2006) 529–541.
[12] J.E. Debreczeni, A.N. Bullock, G.E. Atilla, D.S. Williams, H. Bregman, S. Knapp, E. Meggers, Angew. Chem. Int. Ed. Engl. 45 (2006) 1580–1585.
[13] K.J. Aldred, H.A. Schwanz, G. Li, B.H. Williamson, S.A. McPherson, C.L. Turnbough Jr., R.J. Kerns, N. Osheroff, Biochemistry 54 (2015) 1278–1286.
[14] A. Wohlkonig, P.F. Chan, A.P. Fosberry, P. Homes, J. Huang, M. Kranz, V.R. Leydon, T.J. Miles, N.D. Pearson, R.L. Perera, A.J. Shillings, M.N. Gwynn, B.D. Bax, Nat. Struct. Mol. Biol. 17 (2010) 1152–1153.
[15] I. Turel, J. Kljun, F. Perdih, E. Morozova, V. Bakulev, N. Kasyanenko, J.A. Byl, N. Osheroff, Inorg. Chem. 49 (2010) 10750–10752.
[16] J. Kljun, A.K. Bytzek, W. Kandioller, C. Bartel, M.A. Jakupec, C.G. Hartinger, B.K. Keppler, I. Turel, Organometallics 30 (2011) 2506–2512.
[17] S. Weiss, Z. Altboum, I. Glinert, J. Schlomovitz, A. Sittner, E. Bar-David, D. Kobiler, H. Levy, Antimicrob. Agents Chemother. 59 (2015) 7497–7503.
[18] W. Castro, M. Navarro, C. Biot, Future Med. Chem. 5 (2013) 81–96.
[19] M.P. Lopez-Gresa, R. Ortiz, L. Perello, J. Latorre, M. Liu-Gonzalez, S. Garcia-Granda, M. Perez-Priede, E. Canton, J. Inorg. Biochem. 92 (2002) 65–74.
[20] Z.H. Chohan, C.T. Supuran, A. Scozzafava, J. Enzyme Inhib. Med. Chem. 20 (2005) 303–307.
[21] S.J. Vandecasteele, W.E. Peetermans, A. Carbonez, J. Van Eldere, J. Bacteriol. 186 (2004) 2236–2239.
[22] L.M.M. Vieira, M.V. de Almeida, H.A. de Abreu, H.A. Duarte, R.M. Grazul, A.P.S. Fontes, Inorg. Chim. Acta 362 (2009) 2060–2064.
[23] J. Azema, B. Guidetti, J. Dewelle, B. Le Calve, T. Mijatovic, A. Korolyov, J. Vaysse, M. Malet-Martino, R. Martino, R. Kiss, Bioorg. Med. Chem. 17 (2009) 5396–5407.
[24] M. Suleiman, M. Al-Noaimi, B. Hammouti, S. Radi, T. Ben Hadda, A. Boshaala, I. Warad, Mor. J. Chem. 1 (2013) 29–32.
[25] S. Grgurić-Šipka, M. Al Arabi, M. Alshtewi, D. Jeremić, G.N. Kaluđerović, S. Gómez-Ruiz, Ž. Žižak, Z. Juranić, T.J. Sabo, J. Serb. Chem. Soc. 73 (2008) 619–630.
[26] S. Sersen, J. Kljun, K. Kryeziu, R. Panchuk, B. Alte, W. Korner, P. Heffeter, W. Berger, I. Turel, J. Med. Chem. 58 (2015) 3984–3996.
[27] L. Burke, H. Humphreys, D. Fitzgerald-Hughes, J. Hosp. Infect. 81 (2012) 192–198.
[28] APEX2, v2012.12–0, Bruker AXS Inc., Madison, Wisconsin, USA, 2012.
[29] SADABS, Bruker AXS Inc., Madison, Wisconsin, USA, 2012.
[30] G.M. Sheldrick, Acta Crystallogr. A64 (2008) 112–122.
[31] V. Vichai, K. Kirtikara, Nat. Protoc. 1 (2006) 1112–1116.
[32] E. Forde, H. Humphreys, C.M. Greene, D. Fitzgerald-Hughes, M. Devocelle, Antimicrob. Agents Chemother. 58 (2014) 978–985.
[33] M. Hanif, H. Henke, S.M. Meier, S. Martic, M. Labib, W. Kandioller, M.A. Jakupec, V.B. Arion, H.B. Kraatz, B.K. Keppler, C.G. Hartinger, Inorg. Chem. 49 (2010) 7953–7963.
[34] R.J. Parker, A. Eastman, F. Bostick-Bruton, E. Reed, J. Clin. Invest. 87 (1991) 772–777.
[35] I. Gourdier, M. Del Rio, L. Crabbe, L. Candeil, V. Copois, M. Ychou, C. Auffray, P. Martineau, N. Mechti, Y. Pommier, B. Pau, FEBS Lett. 529 (2002) 232–236.
[36] U.M. Moll, N. Concin, in: G.P. Zambetti (Ed.), The p53 Tumor Suppressor Pathway and Cancer, Protein Reviews, vol. 2, Springer, US 2005, pp. 115–154.
[37] S.M. Post, A. Quintás-Cardama, G. Lozano, in: Z.H. Siddik (Ed.), Checkpoint Controls and Targets in Cancer Therapy, Cancer Drug Discovery and Development, Humana Press, New York 2009, pp. 171–188.
[38] F. Toscano, B. Parmentier, Z.E. Fajoui, Y. Estornes, J.A. Chayvialle, J.C. Saurin, J. Abello, Biochem. Pharmacol. 74 (2007) 392–406.
[39] J.G. Gong, A. Costanzo, H.Q. Yang, G. Melino, W.G. Kaelin Jr., M. Levrero, J.Y. Wang, Nature 399 (1999) 806–809.
[40] G.M. Almeida, T.L. Duarte, P.B. Farmer, W.P. Steward, G.D. Jones, Int. J. Cancer 122 (2008) 1810–1819.
[41] O. Aranha, D.P. Wood Jr., F.H. Sarkar, Clin. Cancer Res. 6 (2000) 891–900.
[42] I. Romero-Canelon, P.J. Sadler, Inorg. Chem. 52 (2013) 12276–12291.
[43] L. Galluzzi, I. Vitale, J.M. Abrams, E.S. Alnemri, E.H. Baehrecke, M.V. Blagosklonny, T.M. Dawson, V.L. Dawson, W.S. El-Deiry, S. Fulda, E. Gottlieb, D.R. Green, M.O. Hengartner, O. Kepp, R.A. Knight, S. Kumar, S.A. Lipton, X. Lu, F. Madeo, W. Malorni, P. Mehlen, G. Nunez, M.E. Peter, M. Piacentini, D.C. Rubinsztein, Y. Shi, H.U. Simon, P. Vandenabeele, E. White, J. Yuan, B. Zhivotovsky, G. Melino, G. Kroemer, Cell Death Differ. 19 (2012) 107–120.
[44] V. Yadav, P. Varshney, S. Sultana, J. Yadav, N. Saini, BMC Cancer (2015), http://dx.doi.org/10.1186/s12885-015-1560-y.